Molecular Rectification

DOI: 10.1002/ange.201306765

Rectification in Nanoscale Devices Based on an Asymmetric Five-Coordinate Iron(III) Phenolate Complex**

*Lanka D. Wickramasinghe, Meeghage Madusanka Perera, Li Li, Guangzhao Mao, Zhixian Zhou, and Cláudio N. Verani**

Rectification consists of an asymmetric flow of electric current. In a macroscopic electrical circuitry, rectifiers, such as vacuum tubes or solid-state diodes, control the mobility of current, enabling it to flow in one direction and preventing reversibility. This directionality is fundamental to the conversion of alternating into direct current. Molecular rectification, which was proposed in the celebrated Aviram–Ratner ansatz,[1] anticipates the feasibility of a current flow in one direction that takes place in an electrode | molecule | electrode junction. Central to this paradigm is the existence of asymmetric molecules that incorporate electron-donor and electron-acceptor moieties, [DA], with an excited state [D^+A^-] of higher, but accessible, energy.[2] Usually, donor and acceptor are separated by a σ- or π-bridge to decrease electronic coupling,[3] and if the requirements are fulfilled, rectification occurs with contributions from Schottky, asymmetric, and/or unimolecular mechanisms. Schottky rectification is based on interfacial dipoles from electrode contact or on covalent bonding between the molecule and the electrode.[4] Asymmetric and unimolecular mechanisms rely on the use of frontier molecular orbitals of the molecule; whereas the former relies on an asymmetric placement of the HOMO or the LUMO in the electrode | molecule | electrode assembly, the latter is based on small HOMO–LUMO gaps that allow for through-molecule current flow.[4a,5] Although experimental distinction between asymmetric and unimolecular contributions can be ambiguous, there is consensus that electroactive molecules with local low symmetry[6] constitute good candidates for this enterprise, and well-documented cases of molecular rectification heavily rely on the formation of high-quality Langmuir–Blodgett (LB) films.[7]

Although it has been shown that self-assembled monolayers of polypyridine–cobalt(II) complexes in octahedral environments[8] can act as single-electron transistors and induce increased resistance (Coulomb blockade) at cryogenic temperatures, the incorporation of transition-metal complexes into electrode | molecule junctions has generally employed symmetric molecules and has been rather slow in development. Examples involve assemblies based on metalloporphyrins,[9] terpyridine–ruthenium(II) complexes,[10] as well as trivalent cobalt[11] and rhodium[12] azo-containing species in octahedral environments that are capable of the symmetric conductance that is relevant for memory-switching devices. An example of rectification based on an octahedral bipyridine/acac–ruthenium(II) system has been reported (acac = acetylacetonate),[13] but the effect of lowering global symmetries around the metal center is yet to be tested.

Our group is engaged in an effort to integrate bioinspired asymmetry principles into new molecular materials, with the aim of developing redox-responsive metallosurfactants with topologies that display unique structural, spectroscopic, and surface patterning behavior. We recently reported on the redox and electronic behavior of five-coordinate complexes where the iron(III) ion is bound to low-symmetry, phenolate-rich, [N_2O_3] environments, and it was shown that geometric and electronic constraints determine the sequence by which the metal and each of the phenolate substituents gets oxidized.[14] Herein, a new iron(III) species [$Fe^{III}\mathbf{L^1}$] (**1**; Scheme 1) is reported. This species shows marked local asymmetries and is based on a newly synthesized amphiphilic and redox-active [N_2O_3] ligand. The complex takes advantage of the presence of the phenylenediamino–metal and phenyl/phenolate moieties that can act as electron-acceptors and electron-donors, respectively. The viability of **1** as a precursor

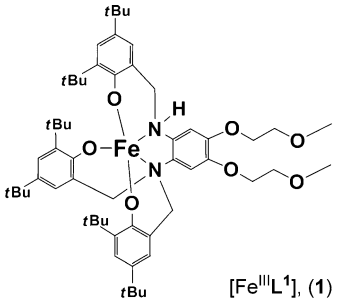

[$Fe^{III}L^1$], (**1**)

Scheme 1. The five-coordinate iron(III) complex [$Fe^{III}\mathbf{L^1}$].

[*] L. D. Wickramasinghe, Prof. C. N. Verani
Department of Chemistry, Wayne State University
5101 Cass Ave, Detroit, MI 48202 (USA)
E-mail: cnverani@chem.wayne.edu
Homepage: http://chem.wayne.edu/veranigroup/

M. M. Perera, Prof. Z. Zhou
Department of Physics & Astronomy, Wayne State University
666 W. Hancock, Detroit, MI 48201 (USA)

L. Li, Prof. G. Mao
Department of Chemical Engineering & Materials Science
Wayne State University
5050 Antony Wayne Dr., Detroit, MI 48202 (USA)

[**] This work was funded by the National Science Foundation through the grants CHE1012413 and CHE0718470 (C.N.V.), ECCS-1128297 (Z.Z.), and CBET-0755654 and CBET-0619528 (G.M.). Dr. S. Shilov (Bruker) is acknowledged for comments on the IRRAS spectra.

Supporting information for this article is available on the WWW under http://dx.doi.org/10.1002/anie.201306755.

for LB films as well as its use in the fabrication of nanoscale rectifying devices are probed.

The ligand $\mathbf{H_3L^1}$ was obtained by treatment of an alkoxylated phenylenediamine, which was synthesized by a multistep method,[15] with 2,4-di-*tert*-butyl-6-(chloromethyl)phenol in presence of triethylamine (Scheme 2). The

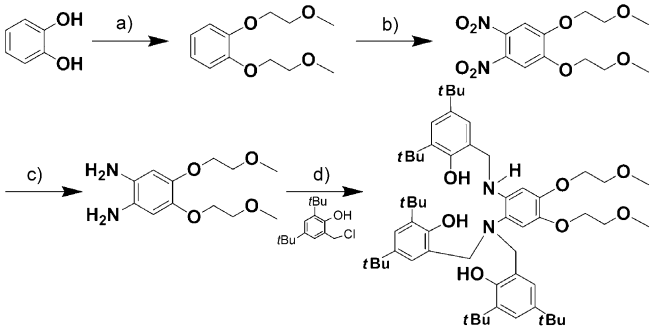

Scheme 2. Multistep synthesis of $\mathbf{H_3L^1}$: a) $CH_3OCH_2CH_2Br$, NaOH, EtOH, reflux, 48 h; b) HOAc, HNO_3, CH_2Cl_2, RT, 72 h; c) Pd/C, hydrazine, EtOH, reflux, 18 h; d) Et_3N, CH_2Cl_2, reflux, 72 h.

ligand $\mathbf{H_3L^1}$ was then treated with anhydrous $FeCl_3$ in presence of sodium methoxide in methanol under inert conditions. Detailed descriptions of the synthetic procedures are available in the Supporting Information. The $[Fe^{III}\mathbf{L^1}]$ (**1**) species was characterized by exact mass spectrometry (Supporting Information, Figure S1), and IR and UV/Vis spectroscopic methods; the results are in excellent agreement with the combustion-analysis results.

The limited information that was obtained by X-ray analysis of the methoxy-substituted analogue (Figure S2) supports the idea that **1** contains an iron(III) metal ion surrounded by three phenolate oxygen atoms and two amine nitrogen atoms of the ligand in a distorted trigonal-bipyramidal geometry. This description is in excellent agreement with experimental and calculated data obtained for species previously described by our group,[16] where average Fe–N and Fe–O bond distances of 2.20 and 1.87 Å were found.[17] Evidence from UV/Vis and IR spectroscopy suggests that **1** retains its amine character, rather than being converted into the equivalent imine species $\mathbf{1^i}$ by ligand oxidation, as usually observed.[16a] This amine/imine conversion will only be observed at the air–water interface and in LB films.

Complex **1** shows well-defined metal- and ligand-centered redox processes in dichloromethane with $TBAPF_6$ as the supporting electrolyte (TBA = tetra-*n*-butylammonium; Figure S3 and Table S1). A cathodic process that appears at approximately −1.49 V versus Fc^+/Fc ($\Delta E_p = 0.18$ V, $|I_{pa}/I_{pc}| = 0.81$; Fc = ferrocene) is assigned to the Fe^{III}/Fe^{II} redox couple, whereas three consecutive phenolate/phenoxyl processes are seen at 0.43 V ($\Delta E_p = 0.09$ V), 0.69 V ($\Delta E_p = 0.12$ V), and 0.9 V versus Fc^+/Fc. The first two processes are quasi-reversible, whereas the third is ill-defined. The electronic origin of these attributions has been investigated in detail, along with the consequences of the lack of orbital degeneracy, which is due to the low symmetry of these five-coordinate species, to redox cycling.[14]

To build nanoscale devices based on LB films of **1**, first the properties of its air–water interface have to be evaluated. Therefore, isothermal compression associated with Brewster angle microscopy (BAM)[18] was used at 23 °C to assess the average area per molecule, the collapse pressure of the monolayers, and the film topology and homogeneity (Figure 1). A good amphiphilic distribution between the

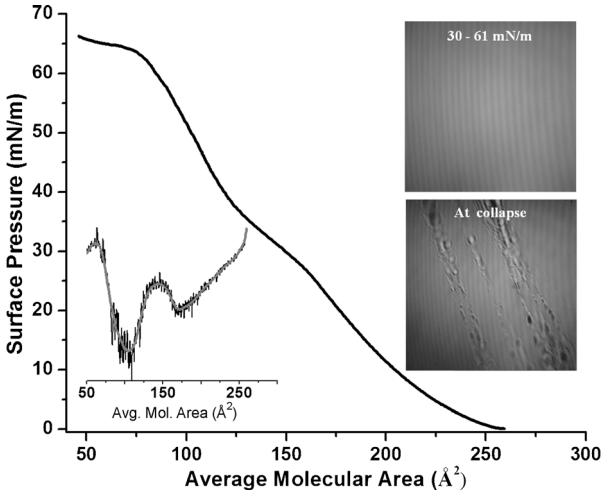

Figure 1. Compression isotherm for complex **1**, its first derivative (curve in inset), and selected BAM micrographs (right; see also the Supporting Information, Figures S5 and S6).

hydrophobic *tert*-butyl groups attached to the phenolate moieties and the hydrophilic methoxyethane chains was found for species **1**. As a consequence, it starts to show intermolecular interactions at the air–water interface at about 260 Å^2 molecule^{-1}. Further compression leads to the formation of a homogeneous film at surface pressures of about 10–20 mN m^{-1}, as observed by BAM images. The formation of Newton rings that are associated with film instability was eventually observed. An apparent phase rearrangement was observed between 25 and 35 mN m^{-1}, which was indicated by a change in the slope of the isotherm, as well as by the absence of Newton rings. The microscopic homogeneity of the film tracked by BAM seems to remain unaltered until ridge formation that is indicative of collapse appears at 63 mN m^{-1}. According to the classic Ries mechanism,[19] collapse involves folding, bending, and breaking of the monolayer. The simplest model for molecular arrangement at the air–water interface suggests that the methoxyethane moiety is submerged in water, whereas the hydrophobic iron–phenolate core remains at the air subphase.

Thus, the approximate area occupied by this core is equivalent to a circle with a radius corresponding to the distance between the outermost *tert*-butyl group of the ligand and the metal ion. In known structures, this distance is approximately 7.9 Å,[14,16b] which results in an area of approximately 200 Å^2 when optimal packing is assumed. Thus, the critical areas should yield a tightly packed film with optimized topology towards the end of the phase transition at 35 mN m^{-1}.

LB films were deposited either as monolayers or multilayers onto glass substrates and studied by UV/Vis spectroscopy, IR reflection/absorption spectroscopy (IRRAS),[20] and by their contact angle, or they were deposited onto quartz and mica and investigated by atomic force microscopy (AFM). This characterization yielded pivotal understanding of the chemical composition, orientation, and thickness of the resulting films. The response of a single monolayer in UV/Vis spectroscopy and IRRAS cannot be detected accurately, and the best results were obtained for films with 25–50 layers on glass. The general π–π* and ligand-to-metal charge transfer (LMCT) features present in the solution spectrum (Figure S4 and Table S2) of **1** are clearly maintained,[14,16a] but obvious changes take place: the intensification of the N–Fe^{III} LMCT band at 330 nm, the hypsochromic shift of the in- and out-of-plane PhO^-–Fe^{III} band at 470 nm, and a new component at approximately 400 nm (Figure S7). This new band is a phenolate-to-azomethine charge transfer associated with the amine/imine conversion of the ligand that takes place at the air–water interface. The **1**→**1**^{i} conversion (Scheme S1) was observed by UV/Vis spectroscopy (Figures S8 and S10) and ESI mass spectrometry (Figures S9 and S11), and by IRRAS on glass at an angle of 30° under *s*-polarized light. In the IR spectrum of **1**^{i}, a new peak at 1583 cm^{-1} that is associated with the C=N group is seen (Figure 2b). As this

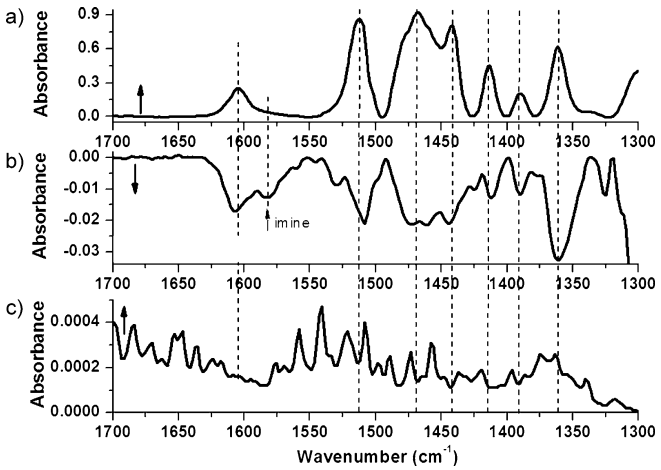

Figure 2. Comparison of the IR spectrum for **1** in KBr (a) and the IRRAS spectra of a 50-layer **1**^{i}–LB film (b) and of moisture at 30° with *s*-polarized light (c).

peak is absent in the bulk IR spectrum of **1** and is not associated with adventitious moisture (Figure 2c), it further validates the intraligand conversion. Other features include the fingerprint region, where peaks that are due to aromatic C=C stretchings (1610–1510 cm^{-1}) and angular -CH_2- and -CH_3 deformations (1360–1470 cm^{-1}) appear (Figure S12).[21] Relevant CH_2 symmetric and antisymmetric stretching vibrations were observed between 2850 to 2920 cm^{-1} and a prominent asymmetric CH_3 feature appears at 2962 cm^{-1}. In previous studies,[20,22] a correlation was drawn between the high intensity of the CH_2 vibrations of alkyl chains and its shifting to lower wavenumbers, as associated with a highly ordered and well-packed film. This relationship requires caution because the CH_2 contribution is smaller than that observed for the CH_3 groups.

Each molecule of **1**^{i} contains 20 methyl groups (18 attached to the phenolates and two attached to the alkoxy chain) and only 6 CH_2 groups (four in the alkoxy chains and two in the methylaminophenolate moiety). Therefore, analysis of the film cannot be based on the intensity of the signals, but must rather be based on the peak position. Indeed, the CH_3 peaks shift from 2954 cm^{-1} in the bulk sample to 2962 cm^{-1} in the film (Figure S13). Considering the average area at collapse reported above, this data corroborates the notion of a well-packed film where the iron/phenolate moiety points outwards. Although the intrinsically complex molecular structure of **1**^{i} prevents us from proposing a tilt angle of alignment, further information about the orientation of the molecules can be gathered by the static contact angle of the compound on glass, which was measured by a KSV CAM 200 goniometer at room temperature. Whereas a value of 7.45° was obtained for the glass substrate alone, the film yielded a value of 85.30°, which confirms its hydrophobic nature.

The morphology of the LB-monolayer of **1**^{i} deposited on mica at surface pressures of 10, 25, 30, 33, and 40 $mN\,m^{-1}$ was measured by AFM. At low surface pressures, the monolayer shows large pinhole defects that become smaller and less frequent as the surface pressure increases (Figure 3a,b; Figure S14). At 33 $mN\,m^{-1}$, the monolayer becomes smooth, which is optimal for nanofabrication. At higher surface pressures, the film becomes rougher owing to material aggregation. In multilayer films, the surface roughness increases with an increasing number of layers (Figure S15 and Table S3), and more particles tend to aggregate to the surface of the film. The thickness of a single monolayer was determined on quartz substrates containing one to fifteen layers by blade-scratching the film and measuring the scratch depth in the tapping mode (Figure 3c; Figure S16 and Table S3). The resulting values yield a linear relationship between the thickness and the number of layers, which indicates homogeneous film deposition (Figure 3d). Each layer is approximately 19 ± 2 Å thick and, based on available crystallographic data for related complexes, the approximate length of **1**^{i} reaches 15–17 Å. With an estimated 12 Å between the catechol-like oxygen atoms and the bulky terminal *tert*-butyl groups,[14,16] these results are in excellent agreement with the notion of a true monolayer. Thus, taking into account the shift in the pronounced CH_3 peak observed by IRRAS, the thickness of the monolayer determined by AFM, and the hydrophobic nature of the film, it is possible to conclude that the LB film of **1**^{i} is composed of well-packed molecules where the alkoxy chains are in contact with the solid substrate and the *tert*-butyl-rich iron/phenolate moiety points outwards at the air–solid interface.

Having gained valuable knowledge about the monolayers at the air–water and air–solid interfaces, we focused on device fabrication. The Langmuir monolayer of **1**^{i} was transferred at 33 $mN\,m^{-1}$ onto a precleaned gold-coated mica substrate to yield a defect-free film. After drying the monolayer for five days under reduced pressure, an Au | **1**^{i}LB | Au device was

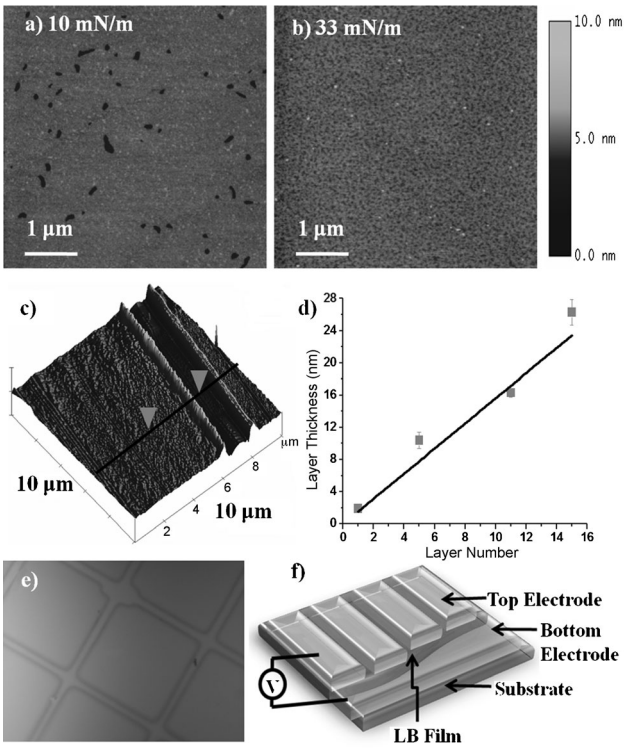

Figure 3. a, b) Surface morphology of the LB monolayers for $\mathbf{1}^{i}$ at 10 mN m^{-1} (a) and at 33 mN m^{-1} (b). c) 3D view of an AFM image of a 15-layer film. d) Layer thickness (nm) versus the number of layers; $\mathbf{1}^{i}$ (■). e) Optical micrograph of the device; image size = 1240 × 930 μm^2. f) Device layout.

built. The top gold electrode was deposited with an Effa-Coater gold sputter by the shadow-masking method using argon as the carrier. Three assemblies with an average of 16 devices each were fabricated, and the current–voltage (*I–V*) characteristics were reproducibly measured in four to five devices per assembly using a Keithley 4200 semiconductor parameter analyzer and a Signatone S-1160 probe station at ambient conditions. A few devices were short-circuited, which was likely to be due to monolayer defects.[6d] An optical micrograph of the fabricated devices and the device layout are shown in Figure 3 e and f. In each of these *I–V* measurements, a higher current was observed in the third quadrant than in the first quadrant. This asymmetric *I–V* that is characteristic of a sharp negative response and a negligible positive response is indicative of rectification behavior, as shown in Figure 4.

The rectification ratio RR (I at $-V_o$/I at $+V_o$)[6d] for the monolayer of $\mathbf{1}^{i}$ varies from 4.52 to 12 between −2 to +2 V and from 2.95 to 36.7 between −4 to +4 V, respectively. Reversing the drain and the source contacts led to a reversed current response, thus demonstrating the retention of the rectification behavior (Figure S17 c). Upon repeating scans, the current drops and the *I–V* behavior displays increased symmetry (Figure S17 e, f). This phenomenon has been observed for organic materials and is tentatively explained by the reorganization of dipole moments in the presence of high electric fields to attain a stable monolayer by decreasing their energy.[6d]

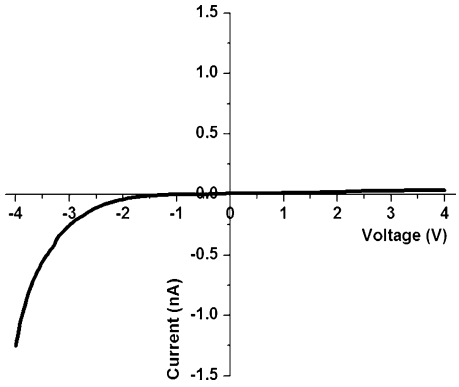

Figure 4. *I–V* diagram for complex $\mathbf{1}^{i}$ (——) from 4 to −4 V.

These results further indicate that the rectifying behavior of the current response is directly associated with the presence of the LB film of $\mathbf{1}^{i}$. Although the exact origin of the rectifying behavior is not certain, unimolecular contribution can be assumed as viable, and a description of the possible [DA] and [D^+A^-] states becomes relevant.[4b,c,5b,6d,23] The redox behavior of **1** in dichloromethane indicates the allowed oxidation states, as the $Fe^{III}\rightarrow Fe^{II}$ reduction was observed, but not the oxidation $Fe^{III}\rightarrow Fe^{IV}$ oxidation. Conversely, the $PhO^-\rightarrow PhO^{\bullet}$ oxidation from phenolate to phenoxyl was observed, whereas the formation of any reduced anionic radical remains unseen for these ligand systems. Thus, it is viable to propose the involvement of Au | $PhO^-\cdots Fe^{III}$ | Au and Au | $PhO^{\bullet}\cdots Fe^{II}$ | Au states, where the LUMO of the ansatz is metal-based, and the HOMO is ligand-centered. Although further considerations will be necessary, DFT calculations for similar systems[14] suggest that partially occupied metal-based SOMOs might be energetically accessible.

In conclusion, we have presented the synthesis and thorough characterization of a new [N_2O_3] ligand and its pentacoordinate iron(III) complex. The balanced amphiphilic nature of **1**, along with imine conversion into $\mathbf{1}^{i}$ at the air–water interface, was pivotal in optimizing the properties of defect-free LB monolayers, as confirmed by spectroscopic and microscopic methods. Furthermore, the asymmetric nature of the complex seemed very useful in designing suitable precursors with current-rectifying properties, as indicated by the *I–V* characteristics of fabricated devices. Asymmetric responses indicative of rectifying behavior were observed for well-ordered LB monolayers of $\mathbf{1}^{i}$ that were sandwiched between two gold electrodes. Considering the molecular structure of $\mathbf{1}^{i}$, along with the associated *I–V* characteristics, it is suggested that the phenolate moiety and the metal center play a role as electron-donors and electron-acceptors in the generation of a directional flow of current. This example of rectification based on an asymmetric coordination complex paves the road towards the investigation of enhanced nanoscale rectifying devices in greater detail. Our laboratories are currently engaged in the optimization of molecular structures that contain new iron(III) complexes with different donating and withdrawing substituents to modulate the $Fe^{III}\rightarrow Fe^{II}$ and the $PhO^-\rightarrow PhO^{\bullet}$ redox

couples, and with predominantly amphiphilic or hydrophobic characters to yield defect-free LB films. The determination of the extent by which redox potentials enhance rectification will allow us to consider the magnitude of asymmetric versus unimolecular contributions. Further results will be reported in due course.

Received: August 1, 2013
Published online: October 14, 2013

Keywords: charge transfer · donor–acceptor systems · molecular rectification · N,O ligands · pentacoordinate iron

[1] A. Aviram, M. Ratner, *Chem. Phys. Lett.* **1974**, *29*, 277 – 283.
[2] a) I. Franco, G. C. Solomon, G. C. Schatz, M. A. Ratner, *J. Am. Chem. Soc.* **2011**, *133*, 15714 – 15720; b) G. J. Ashwell, B. Urasinska-Wojcik, L. J. Phillips, *Angew. Chem.* **2010**, *122*, 3586 – 3590; *Angew. Chem. Int. Ed.* **2010**, *49*, 3508 – 3512; c) W. J. Shumate, D. L. Mattern, A. Jaiswal, D. A. Dixon, T. R. White, J. Burgess, A. Honciuc, R. M. Metzger, *J. Phys. Chem. B* **2006**, *110*, 11146 – 11159; d) A. Troisi, M. A. Ratner, *Nano Lett.* **2004**, *4*, 591 – 595; e) A. Troisi, M. A. Ratner, *J. Am. Chem. Soc.* **2002**, *124*, 14528 – 14529; f) C. Joachim, J. K. Gimzewski, A. Aviram, *Nature* **2000**, *408*, 541 – 548; g) R. M. Metzger, *Acc. Chem. Res.* **1999**, *32*, 950 – 957.
[3] R. M. Metzger, *Chem. Rev.* **2003**, *103*, 3803 – 3834.
[4] a) R. M. Metzger, *J. Mater. Chem.* **2008**, *18*, 4364 – 4396; b) G. J. Ashwell, B. Urasinska, W. D. Tyrrell, *Phys. Chem. Chem. Phys.* **2006**, *8*, 3314 – 3319; c) G. J. Ashwell, A. Mohib, *J. Am. Chem. Soc.* **2005**, *127*, 16238 – 16244; d) Y. Liu, Y. Xu, D. Zhu, *Synth. Met.* **1997**, *90*, 143 – 146; e) Y. Liu, Y. Xu, J. Wu, D. Zhu, *Solid State Commun.* **1995**, *95*, 695 – 698.
[5] a) V. Mujica, M. A. Ratner, A. Nitzan, *Chem. Phys.* **2002**, *281*, 147 – 150; b) M. L. Chabinyc, X. Chen, R. E. Holmlin, H. Jacobs, H. Skulason, C. D. Frisbie, V. Mujica, M. A. Ratner, M. A. Rampi, G. M. Whitesides, *J. Am. Chem. Soc.* **2002**, *124*, 11730 – 11736; c) C. Krzeminski, C. Delerue, G. Allan, D. Vuillaume, R. M. Metzger, *Phys. Rev. B* **2001**, *64*, 085405.
[6] a) N. Nerngchamnong, L. Yuan, D.-C. Qi, J. Li, D. Thompson, C. A. Nijhuis, *Nat. Nanotechnol.* **2013**, *8*, 113 – 118; b) O. Azzaroni, M. Alvarez, A. I. Abou-Kandil, B. Yameen, W. Knoll, *Adv. Funct. Mater.* **2008**, *18*, 3487 – 3496; c) S.-K. Oh, L. A. Baker, R. M. Crooks, *Langmuir* **2002**, *18*, 6981 – 6987; d) R. M. Metzger, B. Chen, U. Hopfner, M. V. Lakshmikantham, D. Vuillaume, T. Kawai, X. Wu, H. Tachibana, T. V. Hughes, H. Sakurai, J. W. Baldwin, C. Hosch, M. P. Cava, L. Brehmer, G. J. Ashwell, *J. Am. Chem. Soc.* **1997**, *119*, 10455 – 10466.
[7] a) A. Jaiswal, D. Rajagopal, M. V. Lakshmikantham, M. P. Cava, R. M. Metzger, *Phys. Chem. Chem. Phys.* **2007**, *9*, 4007 – 4017; b) G. J. Ashwell, B. J. Robinson, M. A. Amiri, D. Locatelli, S. Quici, D. Roberto, *J. Mater. Chem.* **2005**, *15*, 4203 – 4205; c) M.-K. Ng, L. Yu, *Angew. Chem.* **2002**, *114*, 3750 – 3753; *Angew. Chem. Int. Ed.* **2002**, *41*, 3598 – 3601; d) T. Xu, I. R. Peterson, M. V. Lakshmikantham, R. M. Metzger, *Angew. Chem.* **2001**, *113*, 1799 – 1802; *Angew. Chem. Int. Ed.* **2001**, *40*, 1749 – 1752; e) C. P. Collier, G. Mattersteig, E. W. Wong, K. Beverly, J. Sampaio, F. M. Raymo, J. F. Stoddart, J. R. Heath, *Science* **2000**, *289*, 1172 – 1175.
[8] W. Liang, M. P. Shores, M. Bockrath, J. R. Long, H. Park, *Nature* **2002**, *417*, 725 – 729.
[9] J. S. Lindsey, D. F. Bocian, *Acc. Chem. Res.* **2011**, *44*, 638 – 650.
[10] a) J. Lee, H. Chang, S. Kim, G. S. Bang, H. Lee, *Angew. Chem.* **2009**, *121*, 8653 – 8656; *Angew. Chem. Int. Ed.* **2009**, *48*, 8501 – 8504; b) K. Seo, A. V. Konchenko, J. Lee, G. S. Bang, H. Lee, *J. Am. Chem. Soc.* **2008**, *130*, 2553 – 2559.
[11] A. Bandyopadhyay, S. Sahu, M. Higuchi, *J. Am. Chem. Soc.* **2011**, *133*, 1168 – 1171.
[12] N. D. Paul, U. Rana, S. Goswami, T. K. Mondal, S. Goswami, *J. Am. Chem. Soc.* **2012**, *134*, 6520 – 6523.
[13] Y. Lee, S. Yuan, A. Sanchez, L. Yu, *Chem. Commun.* **2008**, 247 – 249.
[14] M. M. Allard, J. A. Sonk, M. J. Heeg, B. R. McGarvey, H. B. Schlegel, C. N. Verani, *Angew. Chem.* **2012**, *124*, 3232 – 3236; *Angew. Chem. Int. Ed.* **2012**, *51*, 3178 – 3182.
[15] a) J. Hu, D. Zhang, S. Jin, S. Z. D. Cheng, F. W. Harris, *Chem. Mater.* **2004**, *16*, 4912 – 4915; b) D. T. Rosa, R. A. Reynolds III, S. M. Malinak, D. Coucouvanis, M. Ali, F. M. MacDonnell, *Inorg. Synth.* **2002**, *33*, 112 – 119; c) M. M. G. Antonisse, B. H. M. Snellink-Ruel, I. Yigit, J. F. J. Engbersen, D. N. Reinhoudt, *J. Org. Chem.* **1997**, *62*, 9034 – 9038; d) E. P. Kyba, E. D. Raymond, C. W. Hudson, A. M. John, S. B. Brown, M. J. McPhaul, L. Liu, A. C. Glover, *J. Am. Chem. Soc.* **1981**, *103*, 3868 – 3875.
[16] a) M. Lanznaster, M. J. Heeg, G. T. Yee, B. R. McGarvey, C. N. Verani, *Inorg. Chem.* **2007**, *46*, 72 – 78; b) M. Lanznaster, H. P. Hratchian, M. J. Heeg, L. M. Hryhorczuk, B. R. McGarvey, H. B. Schlegel, C. N. Verani, *Inorg. Chem.* **2006**, *45*, 955 – 957.
[17] a) L. H. Tong, Y.-L. Wong, S. I. Pascu, J. R. Dilworth, *Dalton Trans.* **2008**, 4784 – 4791; b) A. K. Nairn, R. Bhalla, S. P. Foxon, X. Liu, L. J. Yellowlees, B. C. Gilbert, P. H. Walton, *Dalton Trans.* **2002**, 1253 – 1255; c) M. D. Snodin, L. Ould-Moussa, U. Wallmann, S. Lecomte, V. Bachler, E. Bill, H. Hummel, T. Weyhermüller, P. Hildebrandt, K. Wieghardt, *Chem. Eur. J.* **1999**, *5*, 2554 – 2565.
[18] a) S. Kundu, A. Datta, S. Hazra, *Phys. Rev. E* **2006**, *73*, 051608; b) S. Kundu, A. Datta, S. Hazra, *Langmuir* **2005**, *21*, 5894 – 5900; c) J. Galvan-Miyoshi, S. Ramos, J. Ruiz-Garcia, R. Castillo, *J. Chem. Phys.* **2001**, *115*, 8178 – 8184.
[19] H. E. Ries, Jr., *Nature* **1979**, *281*, 287 – 289.
[20] a) G. Brezesinski, B. Dobner, C. Stefaniu, D. Vollhardt, *Langmuir* **2011**, *27*, 5386 – 5392; b) H. Hamoudi, F. Chesneau, C. Patze, M. Zharnikov, *J. Phys. Chem. C* **2011**, *115*, 534 – 541; c) G. Brezesinski, B. Dobner, C. Stefaniu, D. Vollhardt, *J. Phys. Chem. C* **2011**, *115*, 8206 – 8213; d) L. Wang, A. Cruz, C. R. Flach, J. Pérez-Gil, R. Mendelsohn, *Langmuir* **2007**, *23*, 4950 – 4958; e) Y. Wang, X. Du, L. Guo, H. Liu, *J. Chem. Phys.* **2006**, *124*, 134706.
[21] K. Nakamoto, *Infrared and Raman Spectra of Inorganic and Coordination Compounds, Part B: Applications in Coordination, Organometallic and Bioinorganic Chemistry*, 6th ed., Wiley, Hoboken, **2008**, chap. 1, pp. 1 – 222.
[22] R. J. Lipert, B. D. Lamp, M. D. Porter in *Modern Techniques in Applied Molecular Spectroscopy* (Ed.: F. M. Mirabella), Wiley, New York, **1998**, pp. 83 – 126.
[23] a) G. J. Ashwell, A. Mohib, J. R. Miller, *J. Mater. Chem.* **2005**, *15*, 1160 – 1166; b) G. J. Ashwell, A. Chwialkowska, L. R. H. High, *J. Mater. Chem.* **2004**, *14*, 2848 – 2851.